

First-Principles Study of p-n-Doped Silicon Quantum Dots: Charge Transfer, Energy Dissipation, and Time-Resolved Emission

Jiangchao Chen,[†] Andrew Schmitz,[†] Talgat Inerbaev,[‡] Qingguo Meng,[†] Svetlana Kilina,[§] Sergei Tretiak,^{||} and Dmitri S. Kilin^{*,†}

[†]Department of Chemistry, University of South Dakota, Vermillion, South Dakota 57069, United States

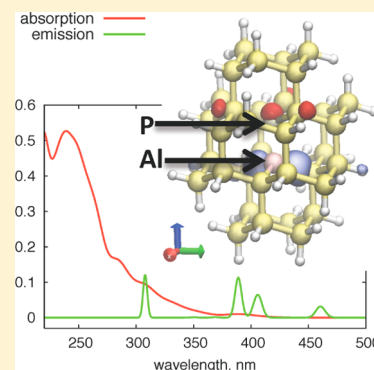
[‡]L.N.Gumilyov Eurasian National University, Munaipassov str. 5, Astana 010008, Kazakhstan

[§]Department of Chemistry and Biochemistry, North Dakota State University, Fargo, North Dakota 58108, United States

^{||}Theoretical Division and Center for Integrated Nanotechnology, Los Alamos National Laboratory, Los Alamos, New Mexico 87454, United States

S Supporting Information

ABSTRACT: Electron–phonon coupling controls nonradiative relaxation dynamics of the photoexcited electron–hole pair in semiconductor nanostructures. Here the optoelectronic properties for Al- and P-codoped silicon quantum dots (QDs) are calculated by combining time-dependent density matrix methodology and ab initio electronic structure methods. The energy-band landscape of the codoped Si QD is elucidated via time evolution of population density distributions in energy and in coordinate space. Multiple nonradiative relaxation pathways result in a specific charge-separated state, where a hole and an electron are localized on Al and P dopants, respectively. Analysis of the simulated nonradiative decay shows that high-energy photoexcitation relaxes to the band gap edge within 10 ps, forming the final charge-transfer state. We also simulate time-resolved emission spectra of the codoped Si QD that reveals optical and IR emissions below the optical band gap. These emission features are attributed to the intraband transitions introduced by doping.



SECTION: Surfaces, Interfaces, Porous Materials, and Catalysis

Being one of the most abundant elements on the Earth, silicon remains the main focus of intense engineering and synthetic efforts in developing new, cheaper-processing nano-sized materials for future technological applications. Thus, crystalline silicon quantum dots have well-studied electronic and optical properties^{1–4} and exhibit technological potentials for photovoltaic devices.^{5–7} Silicon nanowires (SiNWs)^{8,9} have recently found many promising applications in electronic devices, waveguides, and solar cells.^{10–12} Most of the photophysical properties important for these applications can be tuned by p- and n-doping of silicon nanostructures. In such doped systems, the p-n junction governs conditions for electron transfer, the efficiency of which is the key factor in energy-conversion materials. As such, elucidating electron-transfer pathways together with energy losses due to lattice-induced charge-carrier relaxation and their dependence on doping is critical for optimizing an efficiency of Si-based optoelectronic and photovoltaic devices. For example, excited-state energy relaxation of SiNW with axial arrangement of p-n junctions¹³ determines the carrier lifetime,^{14–16} and photoluminescence efficiency.^{17–20} Femtosecond pump–probe imaging has been recently applied to get insights into charge-carrier recombination in SiNW;^{19,20} however, interpretation of time-resolved emission spectra is challenging because of the “dark” character of electronic states of indirect-bandgap semiconductors, such as silicon. As such, theoretical insights into pathways and mechanisms of relaxation dynamics and photoemission in silicon

nanostructures could elucidate ways for controlling these processes and help in rational design of Si-derived materials.

Various first-principle approaches beyond Born–Oppenheimer approximations have been developed to describe such hot carrier relaxation dynamics in different molecules,^{21–24} solids,^{25,26} and nanostructures,^{27–29} including surface-hopping technique³⁰ combined with methods ranging from density functional theory (DFT)^{27–29} to semiempirical configurationally interaction (CI) approaches^{31–34} and the multilevel Redfield theory.^{35–43} Our previous computational modeling of various silicon nanostructures (including elongated codoped silicon QDs) based on DFT electronic structure calculations and linear response time-dependent DFT (TDDFT) simulations of excited states allowed for a detailed analysis of their optical properties,^{44–47} while relaxation rates in these systems have been investigated based on the phenomenological Redfield theory.⁴⁸

In the present work, we extend our simulations of the relaxation rates of photoexcited electrons and holes in Si QDs with Al and P dopants by applying an ab initio treatment of the electronic states, when the underlying nonadiabatic transitions are accompanied by the respective vibrational dynamics. Such calculated

Received: April 10, 2013

Accepted: June 2, 2013

Published: August 15, 2013

on-the-fly nonadiabatic couplings are then used as parameters to the Redfield theory, providing dynamics of carriers and allowing for analysis of multiple nonradiative relaxation pathways in codoped Si QDs. The observed ultrafast electron–phonon dynamics following photoexcitation is found to be controlled by doping concentration and location. In addition, we simulate, for the first time, the time-resolved emission spectra of the codoped Si QD: the observable that can be directly compared with experimental data. Our simulations provide information on the nature and lifetime of emission states in doped nanomaterials. Because interpretation of time-resolved data is a challenging experimental task, our calculations could be valuable in the analysis of pump–probe spectroscopy measurements.

We focus our modeling on Al- and P-codoped silicon quantum dot (QD) with a composition formula $\text{Si}_{36}\text{Al}_1\text{P}_1\text{H}_{42}$. The codoped QDs are elliptical and elongated in the $\langle 111 \rangle$ direction, along which the dopant atoms are spread. The undoped Si QD of the composition $\text{Si}_{38}\text{H}_{42}$ is used for a reference. An electronic structure of these clusters has been calculated using DFT^{49,50} with the Perdew–Burke–Ernzerhof (PBE) functional,⁵¹ as implemented in the VASP software package.⁵² In this software, the valence electrons are treated explicitly, while the core electrons are described with PAW pseudopotentials.⁵³ All calculations are done in the plane-wave basis. Several electronic properties have been extracted from these calculations, including the energy gap between the respective Kohn–Sham highest occupied (HO) and lowest occupied (LU) molecular orbitals, the electronic density of states (DOS), the excitation lifetime, and the absorption spectrum.

The absorption spectra are calculated as

$$\alpha(\omega) = \sum_{I=ij} f_I \delta(\hbar\omega - \hbar\omega_I) \quad (1)$$

where the double index $I = ij$ runs over all possible transitions between occupied i and valence j Kohn–Sham energy levels with transition frequency $\hbar\omega_I$. Each Dirac delta function δ is weighted by the oscillator strength f_I corresponding to the transition. (See the details in the Supporting Information.) Each resonance has been further broadened by 0.05 eV to model the finite spectral width of the peaks.

The question of validity of a single-particle approach to the excited state in QDs has been addressed in several investigations.⁵⁴ The studies of CdSe QDs show that excitonic effects lead to a systematic red shift of transition energies (of ~ 0.3 eV), while not changing the shape and profile of the spectra. The reason for such behavior is that the quantum confinement effect in QD ensures that the electron and hole kinetic energies ($T \approx 1/R^2$) dominate their electrostatic interaction ($E_{\text{ex}} \approx 1/R$), as can be derived from the effective mass theory.⁵⁵ As a result, the optical spectra of QDs are qualitatively represented by the independent electron and hole picture.⁵⁶ To confirm the validity of this approach in the case of Si QD, we have compared optical transitions obtained from a single-particle approach used in our work with those calculated by linear response TD-DFT, which incorporates electron–hole corrections. (See the details in the Supporting Information.) As shown in Figure S1 in the Supporting Information, TD-DFT and DFT spectra of doped and pristine $\text{Si}_{38}\text{H}_{42}$ exhibit the same features shifted by a constant energy offset of ~ 0.6 eV independent of transition energy, while the spectral shape stays unchanged. Thus, similar to reported results for CdSe QDs,⁵⁶ a single-particle approach is appropriate for qualitative description of the optical spectra of Si quantum dots.⁵⁷

By analogy to the absorption spectra, we further evaluated the spectral density of emission from the density matrix $\rho_{ij}(t)$ corresponding to excited, nonequilibrium states as

$$E(\omega, t) = \sum_{j>i} f_{ij} \delta(\hbar\omega - \hbar\omega_{ij}) \{ \rho_{jj}(t) - \rho_{ii}(t) \} \quad (2)$$

$$E^{\text{int}}(\omega) = \int_{-\infty}^0 dt E(\omega, t)$$

Here f_{ij} , $\hbar\omega_{ij}$, and ω stand for an oscillator strength, Kohn–Sham orbital energy difference, and emission frequency, respectively, and $i(j)$ labels virtual (occupied) orbitals. The information about time evolution of density matrix elements is a critical component for computing time-resolved spectral probes, charge density distribution, as well as rates of energy dissipation and charge transfer.

To simulate time-dependent electronic properties, we further performed molecular dynamics modeling using the VASP package for up to 1 ps trajectory at ambient temperature. In our approach, we neglect the vibrational reorganization of the excited state, assuming that the geometry of the excited state is negligibly changed upon photoexcitation due to rigidity of inorganic structure. This approximation is justified by relatively small Huang–Rhys factors in silicon, as has been experimentally and theoretically shown in several reports.^{58–60} Extended discussion on this question is provided in the Supporting Information. Following the procedure described elsewhere,^{26,61,62} this provides us with variations of DFT Hamiltonian, Kohn–Sham energies, and nonadiabatic couplings between electronic levels computed on-the-fly along the nuclear trajectory. Subsequently, the time dependence for the density matrix (see the Supporting Information) is computed for a specific initial excitation $\rho_{ij}^{(a,b)}(t=0)$, where initially an electron is promoted from an orbital a to an orbital b by solving the equation of motion for the reduced density matrix for electronic degrees of freedom

$$\dot{\rho}_{jk} = -\frac{i}{\hbar} \sum_l (F_{jl}\rho_{lk} - \rho_{jl}F_{lk}) + \left(\frac{d\rho_{jk}}{dt} \right)_{\text{diss}} \quad (3)$$

where F_{ij} in the first term is either one-electron Fock or Kohn–Sham Hamiltonian. The second term in eq 3 $(d\rho_{jk}/dt)_{\text{diss}} = \sum_{lm} R_{jklm}\rho_{lm}$ represents dissipative electronic transitions facilitated by thermal fluctuations of the lattice ions through nonadiabatic couplings. A time average of the autocorrelation function of the electron-to-lattice nonadiabatic couplings provides coefficients of dissipative electronic transition quadratic operator R_{jklm} that enter into the equation of motion eq 3 for the electronic degrees of freedom. This approach describes electron–phonon relaxation phenomena and allows for calculation of dynamics of electronic charge distribution. This model implies the following approximations: the ions are considered to be point charges, the lattice vibrations abruptly equilibrate with a thermostat, the coupling autocorrelation function decays instantaneously leading to the Markov approximation, the vibrational reorganization is neglected, and the excited- and ground-state potential-energy surfaces are assumed to have the same profiles (classical path approximation).

Figure 1a shows a schematic representation of ground-state electronic structure of codoped Si QDs emerged from DFT electronic structure calculations. The dopants Al and P atoms create new states in the bandgap area near the CB minimum and the VB maximum, respectively. There are six different representative optical transitions illustrated in Figure 1a. Among them, four excitations

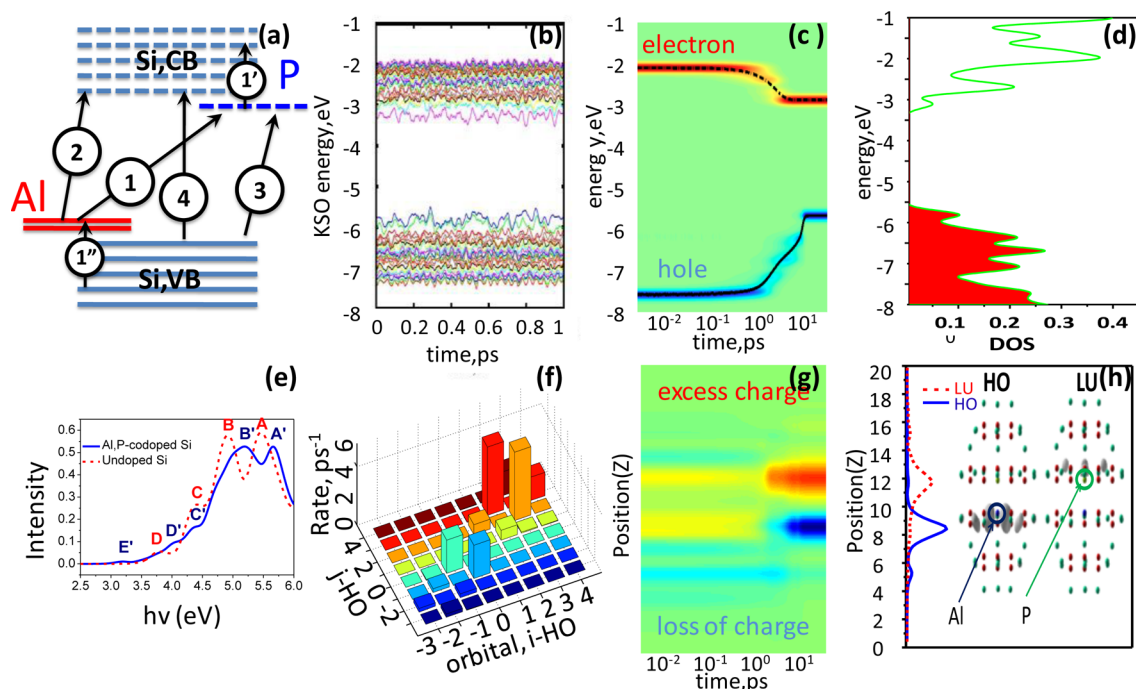


Figure 1. (a) Schematic representation of electronic structure of Al and P codoped Si QD in its ground state. Solid (dashed) lines represent occupied (empty) orbitals. Color-coding symbolizes the assignment of orbitals to different elements. Arrows symbolically represent different transitions: Interband transitions are labeled by 1, 2, and 3 and intraband transitions are labeled by 1' and 1''. (b) Time evolution of KS orbital's energy along the 1 ps molecular dynamics trajectory. (c) Iso-contours of the population $\Delta n^{(a,b)}(\epsilon, t)$ providing the dynamics of electron (red) and a hole (blue) after photoexcitation (peak A') in the codoped silicon QD; green corresponds to zero population. (d) Equilibrium density of states (DOS) of the codoped Si QD. (e) Calculated absorption spectra of the codoped (blue) and undoped (red) QDs. (f) Examples of absolute values of Redfield tensor elements $|R_{ijij}|$ used to simulate photoexcited dynamics. (g) Dynamics of spatial distribution of charge population $\Delta n^{(a,b)}(z, t)$. (h) Partial charge density of HO and LU orbitals projected on the Z axis and their 3D iso-surfaces (gray clouds) for codoped Si QD. Blue, green, ocean green, and red spheres stand for Al, P, H, and Si atoms, respectively.

signify interband transitions including dopant to dopant (transition 1), dopant to Si (transition 2), Si to dopant (transition 3), and Si to Si (transition 4). The remaining two processes represent intraband transitions inside the conduction band (CB) (transition 1') and inside the valence band (VB) (transition 1''). The dopants change the electronic structure of the QD and further influence its optoelectronic properties, including absorption spectra, charge transfer, etc. The electronic energy scale in the first row of Figure 1 is the same for all panels, which gives us a consistent comparison.

Figure 1b shows evolution of the KS orbital energies along 1 ps adiabatic dynamics trajectory calculated at room temperature. Thermal lattice vibrations significantly influence the sway of their energies during molecular dynamics. The electron-to-lattice interaction enables the energy redistribution between electronic and nuclear subsystems, a process going beyond the Born–Oppenheimer approximation. Two orbitals (blue and light green) near the gap at the edge of the VB with energies around -6 eV are contributed by the Al dopant. In addition, one orbital near the edge of the CB (about -3 eV) is attributed to the P dopant. It is interesting to note that the fluctuations of dopants' orbitals tend to have larger amplitudes of orbital energy variation than those of Si-host orbitals, as shown in Figure 1b. This is an indirect sign of more localized character of dopant orbitals than the bulk-like Si delocalized states. This statement is supported by Figure 1h, displaying the HO and LU partial charge densities projected onto the z axis. Figure 1h directly illustrates the significant localization of HO on Al and LU on P dopant atoms with a small portion delocalized over Si

atoms. One can provide the following explanation of larger oscillation of localized orbitals: If an orbital is localized around some ion, then changes in a motion of this atom should lead to significant perturbations of the electronic density of this state that results in noticeable changes in its electronic energy during dynamics. In contrast, if an orbital is delocalized so that the corresponding charge density distribution is nonzero in the vicinity of each nucleus in the crystal lattice, thermal fluctuations of nuclei motion provide contributions of almost random amplitude and phase into the energy of such orbital.^{63,64} An average of such contributions adds up in a destructive way and hence results in small changes of the electronic energy. The situation is different for localized orbitals: Being dependent on distortion of only one or a few ions, the average contribution of nucleus motion is constructive and the relevant orbital energies get substantial fluctuations. Because the orbitals contributed by Al and P dopants are localized around a few atoms, it is expected that these states should strongly fluctuate. In the undoped model, the orbitals are very delocalized and show smaller fluctuations.

Figure 1d shows the resulting DOS of Kohn–Sham orbitals calculated using an electronic structure at equilibrium (ground-state optimal geometry) and 0.05 eV empirical broadening parameter for each state. As expected, the orbitals associated with dopants appear as additional features near the bandgap in the codoped Si QD. Namely, the Al (III group element) dopant contributes to the new HO at $\epsilon(\text{HO}) = -5.7$ eV, whereas the P (V group element) dopant brings forward LU at $\epsilon(\text{LU}) = -3.1$ eV. As such, doping narrows the bandgap of semiconductor

cluster to ~ 2.3 eV, denoted here as p-n junction, where p (positive) and n (negative) refer to Al and P dopants, respectively. Such electronic structure already suggests that if photoexcitation of codoped Si QD relaxes to HO and LU orbitals, then the final stage represents a charge-separated state with an electron and a hole localized on P and Al dopants, respectively.

The calculated absorption spectra of codoped and undoped QDs are shown in Figure 1e. The high intensity peaks signify transitions with the largest oscillator strengths. The spectra show features (A/A', B/B', C/C', and D/D') similar for both codoped Si and undoped Si clusters, owing to transitions between Si-based orbitals. In addition, the codoped cluster has a unique lower-intensity feature E', attributed to the dopants. Moreover, the absolute values of energies of features A', B', C', and D' are shifted compared with the undoped case, which is also due to the host-doping interaction.

To simulate photoexcitation dynamics (time evolution of electron-hole pairs of orbitals), we first extract the Redfield tensor R_{ijij} from our DFT calculations. Absolute values of selected elements of R_{ijij} are shown Figure 1f. The diagonal line (from the left bottom corner to the right top corner) corresponds to very small transition rates, which are not physically meaningful, representing transitions between the same orbital. Only several transition rates along the subdiagonal lines are nonvanishing, indicating that nonradiative transitions are most probably occur between the nearest neighboring orbitals $|i - j| = 1$. Similar results on the dominant contribution of the phonon-mediated transitions between the nearest neighboring states have been obtained for CdSe and PbSe QDs.²⁷⁻²⁹ For the doped Si QD, these transitions can be symbolically arranged in three types: (i) intraband electron relaxation in the CB, shown in the positive quadrant ($i > \text{HO}, j > \text{HO}$), (ii) intraband hole relaxation in the VB, shown in the negative quadrant, ($i \leq \text{HO}, j \leq \text{HO}$), and (iii) interband nonradiative electron-hole recombination processes, shown in the cross-quadrants ($i \leq \text{HO}, j > \text{HO}$) and ($i > \text{HO}, j \leq \text{HO}$). We observe that the transition rates for electrons are higher than those for holes (see Table 1), ascribed to stronger nonadiabatic couplings in the CB compared with that in the VB.⁶⁵

If the cluster is irradiated by a steady light with the frequency $\Omega = (\epsilon_b - \epsilon_a)/\hbar$, an electron can be excited from the state a in the VB to the state b in the CB. Notably, such photoexcitation could be composed of multiple electron hole pairs. Here we created the photoexcited electron-hole pair by promoting an electron from $a = \text{HO-30}$ to $b = \text{LU+7}$, which corresponds to the absorption feature A' in the spectrum of the codoped QD, with transition energy of 5.65 eV. This is the dominant optically active state computed for this cluster. Using previously developed formalism for optical properties,^{44,45,47,48,66,67} we further model excitation dynamics, that is, nonradiative relaxation of the electron and hole states down to the LU and HO orbitals, respectively, occurring due to nonadiabatic electron-phonon processes. Such relaxation has been recently experimentally investigated in the codoped QDs.^{17,18} Our simulation results shown in Figure 1c summarize evolution of electron and hole states starting from the photoexcited peak A'. Displayed are the iso-contours of the population $\Delta n^{(a,b)}(\epsilon, t)$ obtained from eq SI-17 (Supporting Information), with red (blue) color indicating large gain (loss) of charge density with respect to the equilibrium distribution. The input orbital energies and their population dynamics were provided by ab

Table 1. Analysis of Dynamics of Photoexcited Electron-Hole Pairs Corresponding to the Different Peaks in the Absorption Spectra in the Co-Doped and Undoped Si QDs^a, Presented in Figure 1e.

absorption peak	undoped Si QD					co-doped Si QD				
	A	B	C	D	A'	B'	C'	D'	E'	
transition energy (eV)	5.4615	4.9170	4.4115	3.8085	5.6596	5.1835	4.3874	4.0900	3.1948	
absorption density	0.5909	0.5777	0.2661	0.0550	0.0526	0.5271	0.1678	0.1040	0.0100	
hole orbital (a)	75=HO-22	83=HO-14	97=HO	87=HO-10	67=HO-30	67=HO-30	97=HO	95=HO-2	97=HO	
electron orbital (b)	113=LU+15	109=LU+11	120=LU+22	98=LU	105=LU+7	100=LU+2	124=LU+26	110=LU+12	102=LU+4	
K_{el} (ps ⁻¹)	0.9946	1.0351	0.8361	0	0.6413	1.4977	0.4686	0.6805	0.8373	
K_{hole} (ps ⁻¹)	0.4155	0.7804	0	0.2881	0.1098	0.1098	0	1.7385	0	
$K_{el} + K_{hole}$ (ps ⁻¹)	1.4101	1.8155	0.8361	0.2881	0.7511	1.6075	0.4686	2.4190	0.8373	

^aEnergy dissipation rates k_{el} and k_{ho} are computed according to eq SI-15 (Supporting Information).

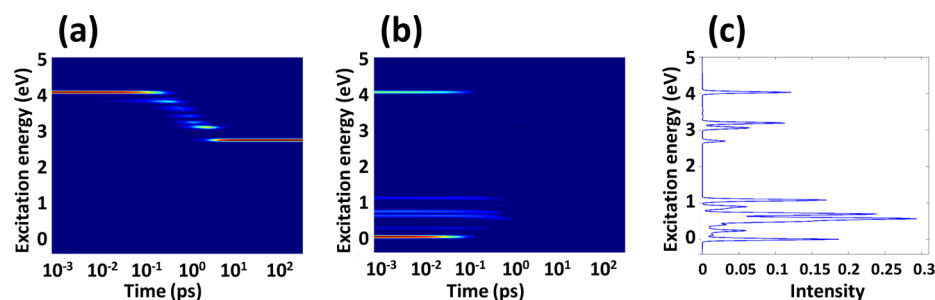


Figure 2. Simulated photoexcited dynamics after excitation at 4.09 eV (peak D' Figure 1e) of the codoped QD. (a) Dynamics of the exciton (electron–hole pair) energy dissipation with time. Colors correspond to the population scaled accordingly to the rainbow order: red stays for maximum population and navy blue for zero population. (b) Calculated time-resolved emission spectrum. Colors correspond to the intensity (oscillator strength) of transition scaled accordingly to the rainbow order: red stays for maximum intensity and navy blue for zero. (c) Integrated emission spectrum.

initio electronic dynamics calculations of the models of codoped $\text{Si}_{36}\text{Al}_1\text{P}_1\text{H}_{42}$.

Figure 1c illustrates that nonradiative internal conversion of photoexcited electron and hole completes within 10 ps. In Figure 1g, we further analyze the evolution of the nonequilibrium charge density distribution projected onto the z direction, calculated with eq SI-28 (Supporting Information). Concomitant to Figure 1c, this picture shows that an electron and a hole reach the LU and HO orbitals localized mainly on the P and Al dopants, respectively. Notably, the electron nonradiative relaxation is faster compared with the hole relaxation, possibly because of the two reasons: (i) the energy of the excited electron orbital is much closer to the band edge compared with that of the hole and (ii) the electron–phonon couplings are stronger than hole–phonon couplings.

Table 1 summarizes our computational results on the energy dissipation and charge-transfer process for different electron–hole excitations ($a \rightarrow b$), corresponding to various peaks in the absorption spectra (Figure 1e) of codoped and undoped clusters.⁴⁸ Different values of energy dissipation rates K_{el} , K_{ho} , and $K_{\text{ex}} = K_{\text{el}} + K_{\text{ho}}$ are computed according to eq SI-25 (Supporting Information). The dissipation rates for electrons in the undoped QD approximately follow the trend, often referred to as “band gap law”. Specifically, relaxation occurs faster for smaller values of an average portion of energy, dissipated in a single event, $\langle \Delta E \rangle = (E(0) - E(\infty))/N_{\text{bands}}$, where N_{bands} stands for the number of individual relaxation steps experienced by the carrier during relaxation pathway. This observation agrees well with the results previously reported for spherical Si-QDs treated by surface-hopping computational technique.⁶⁵ Overall, the calculated net internal conversion rates after photoexciting the dominating absorbance peaks (A/A', B/B', and C/C' (Figure 1e)) are slightly slower in the codoped QD compared with the respective rates in the undoped cluster, as compared in Table 1. The exception is the fast relaxation rate for the initial excitation near the Si–Si bandgap (peak D') in the codoped QD. In contrast with the undoped QD, these peak involves both electron and hole transitions, with holes relaxing very fast from HO-2 to HO. Because of hybridization of orbitals on Si and Al atoms, hole states are strongly coupled to phonons and exhibit ultrafast formation of final charge-transfer state on the Al and P dopants' orbitals.

To study in details dynamics of radiative and nonradiative energy dissipation, we now focus on the photoexcitation with the energy of 4.09 eV promoting an electron from HO-2 to LU+12, which corresponds to the C' peak in absorbance spectra. Figure 2a clearly demonstrates that electronic energy dissipation

via the lattice vibrations predominantly occurs between about 0.1 and 4 ps and then stays at the edge of the band gap for longer than 100 ps. Using eq 2 (also see eq SI-11 in the Supporting Information), we have computed time-resolved emission spectrum following the instantaneous photoexcitation at transition energy of 4.09 eV, as displayed in Figure 2b. An emission signal at the range 4.09 eV, which corresponds to the parent interband absorption from VB to CB (peak C'), disappears within 0.1 ps, reflecting the beginning of the vibrational relaxation. Transitions at energy of ~ 3.3 eV seen in Figure 2a at a time interval of 1 to 2 ps have very weak photoluminescence and are not seen in Figure 2b. The intensity of this component is weaker than other transitions because the excitation is relaxing further down in energy toward charge-transfer dark states. Interestingly, there are five additional intraband emission features at energies less than 1.5 eV. These bands are absent in the absorption spectrum. Because the bandgap of codoped Si QD is more than 2 eV, these emission signals correspond to the *intraband* transitions CB to CB or VB to VB (1' and 1'' transitions in Figure 1a) for the photoexcited electron or hole. These radiatively allowed transitions with the energies smaller than the band gap can be observed in ultrafast time-resolved pump–probe spectroscopies. Figure 2c presents the respective integrated emission spectrum of the codoped Si QD after 4.09 eV photoexcitation. The emission peaks at 4.09 and 0 to 1 eV are consistent with the features in Figure 2b. However, the emission features around 3 eV (Si–Si interband photoluminescence), which are very weak and invisible in Figure 2b, clearly appear in the integrated emission plot. These excitations are activated in the later stages of the dynamics (after 1 ps) and stay active for a longer period of time (up to 6 ps), providing a noticeable contribution to the integrated emission. Previously, photoluminescence of B- and P-codoped Si QDs has been experimentally detected at transition energies below the band gap of Si.^{17,18} We attribute these optical transitions to the hydrogen-like states of the shallow dopants.⁶⁸

In summary, the optoelectronic properties and nonadiabatic photoexcited dynamics of p-n doped and undoped Si QD are modeled using theoretical technique combining density matrix formalism and *ab initio* electronic structure calculations. Our simulations provide detailed information on absorption spectra, nonradiative relaxation, and time-resolved photoluminescence spectra in both codoped and undoped Si clusters. Overall, the fundamental Si–Si cluster bandgap is tuned by quantum confinement in both systems. However, compared with the undoped cluster, Al and P dopants introduce new states near the bandgap, which are spatially localized on the dopant atoms. Our results

demonstrate that transitions between those bands contribute to the absorption and emission spectra. For instance, the absorption spectrum of the codoped QD reveals an additional low-energy peak arising from the dopant transitions compared with the spectrum of the undoped model. Simulated time-resolved emission spectra of the codoped QD contain short-lived interband together with intraband transitions. Emission with energies larger than the optical bandgap is ascribed to the interband transitions between the host silicon states. Our simulations also revealed optical and IR emissions below the optical band gap. These emission features are attributed to the intraband transitions introduced by doping. Similar emission with energies below the band gap has been experimentally detected in B- and P-codoped Si QDs,^{17,18} and our simulations help to elucidate the nature of such transitions. Photoexcited electron and hole relax nonradiatively within 10 ps, when 1.5 to 3 eV of electronic energy is being transferred to the heat (lattice vibrations). The initially delocalized charge density then evolves to the lowest excited electronic state, which has charge-separated character (i.e., an electron and a hole reach LU and HO states localized mostly on Al and P atoms, respectively). Our computational modeling provides detailed analysis of the optoelectronic properties of Si QD with p-n dopants, which could be helpful for improving nanostructured semiconductor materials for photovoltaic applications.

■ ASSOCIATED CONTENT

● Supporting Information

Details of the model used in the calculations, validity of single-particle Kohn-Sham approach to excitations, calculated photon absorption spectra for the undoped and co-doped with Al and P atoms Si-quantum dots, discussion of ground-state nuclear trajectory approximation, and schematic representation of potential energy surfaces for which one can apply classical path approximation. This material is available free of charge via the Internet at <http://pubs.acs.org>.

■ AUTHOR INFORMATION

Corresponding Author

*E-mail: Dmitri.Kilin@usd.edu. Phone: (605) 677-7283. Fax: (605) 677-6397.

Notes

The authors declare no competing financial interest.

■ ACKNOWLEDGMENTS

This work was supported financially by the South Dakota Governor's Office of Economic Development, NSF award EPS0903804, DOE, BES-Chemical Sciences, NERSC Contract No. DE-AC02-05CH11231, allocation Awards 85213 and 86185 "Computational Modeling of Photocatalysis and Photoinduced Charge Transfer Dynamics on Surfaces", Computational resources of USD High Performance Computing facilities operated by Douglas Jennewein, and the Dean's Opportunity Fund of the College of Arts and Sciences, University of South Dakota are acknowledged. T.I. acknowledges Ministry Science and Education of Republic of Kazakhstan for financial support through Contract No. 556 of April 15, 2013. S.K. acknowledges support of the U.S. Department of Energy Early-Career Grant DE-SC008446. D.K. thanks Ivan Mikhaylov for discussions and help in estimating exciton binding energy in Si nanostructures. We also acknowledge support of Center for Integrated Nanotechnology (CINT) and Center for Nonlinear Studies

(CNLS) at Los Alamos National Laboratory (LANL). LANL is operated by Los Alamos National Security, LLC, for the National Nuclear Security Administration of the U.S. Department of Energy under contract DE-AC52-06NA25396.

■ REFERENCES

- (1) Chen, X.; Pi, X.; Yang, D. Bonding of Oxygen at the Oxide/Nanocrystal Interface of Oxidized Silicon Nanocrystals: An Ab Initio Study. *J. Phys. Chem. C* **2010**, *114*, 8774–8781.
- (2) Martínez, A.; Alonso, J. C.; Sansores, L. E.; Salcedo, R. Electronic Structure of Silicon Nanocrystals Passivated with Nitrogen and Chlorine. *J. Phys. Chem. C* **2010**, *114*, 12427–12431.
- (3) Lehtonen, O.; Sundholm, D. Density-Functional Studies of Excited States of Silicon Nanoclusters. *Phys. Rev. B* **2005**, *72*, 085424.
- (4) Brus, L. Luminescence of Silicon Materials - Chains, Sheets, Nanocrystals, Nanowires, Microcrystals, and Porous Silicon. *J. Phys. Chem.* **1994**, *98*, 3575–3581.
- (5) Würfel, P. *Physics of Solar Cells*; Wiley-VCH: Weinheim, Germany, 2005.
- (6) Green, M. A. Recent Developments in Photovoltaics. *Sol. Energy* **2004**, *76*, 3–8.
- (7) Goetzberger, A.; Hebling, C.; Schock, H.-W. Photovoltaic Materials, History, Status and Outlook. *Mater. Sci. Eng., R* **2003**, *40*, 1–46.
- (8) Westwater, J.; Gosain, D. P.; Tomiya, S.; Usui, S.; Ruda, H. Growth of Silicon Nanowires via Gold/Silane Vapor-Liquid-Solid Reaction. *J. Vac. Sci. Technol., B* **1997**, *15*, 554–557.
- (9) Wu, Y. Y.; Yang, P. D. Direct Observation of Vapor-Liquid-Solid Nanowire Growth. *J. Am. Chem. Soc.* **2001**, *123*, 3165–3166.
- (10) Pauzauskis, P. J.; Yang, P. Nanowire Photonics. *Mater. Today* **2006**, *9*, 36–45.
- (11) Thelander, C.; Agarwal, P.; Brongersma, S.; Eymery, J.; Feiner, L. F.; Forchel, A.; Scheffler, M.; Riess, W.; Ohlsson, B. J.; Gosele, U.; et al. Nanowire-Based One-Dimensional Electronics. *Mater. Today* **2006**, *9*, 28–35.
- (12) Huang, Y.; Lieber, C. M. Integrated Nanoscale Electronics and Optoelectronics: Exploring Nanoscale Science and Technology Through Semiconductor Nanowires. *Pure Appl. Chem.* **2004**, *76*, 2051–2068.
- (13) Hoffmann, S.; Bauer, J.; Ronning, C.; Stelzner, T.; Michler, J.; Ballif, C.; Sivakov, V.; Christiansen, S. H. Axial p-n Junctions Realized in Silicon Nanowires by Ion Implantation. *Nano Lett.* **2009**, *9*, 1341–1344.
- (14) Seo, M. A.; Dayeh, S. A.; Upadhyay, P. C.; Martinez, J. A.; Swartzentruber, B. S.; Picraux, S. T.; Taylor, A. J.; Prasankumar, R. P. Understanding Ultrafast Carrier Dynamics in Single Quasi-One-Dimensional Si Nanowires. *Appl. Phys. Lett.* **2012**, *100*, 071104.
- (15) Jung, Y. W.; Vacic, A.; Perea, D. E.; Picraux, S. T.; Reed, M. A. Minority Carrier Lifetimes and Surface Effects in VLS-Grown Axial p-n Junction Silicon Nanowires. *Adv. Mater.* **2011**, *23*, 4306–4311.
- (16) Mohite, A. D.; Perea, D. E.; Singh, S.; Dayeh, S. A.; Campbell, I. H.; Picraux, S. T.; Htoon, H. Highly Efficient Charge Separation and Collection across in Situ Doped Axial VLS-Grown Si Nanowire p-n Junctions. *Nano Lett.* **2012**, *12*, 1965–1971.
- (17) Fujii, M.; Yamaguchi, Y.; Takase, Y.; Ninomiya, K.; Hayashi, S. Control of Photoluminescence Properties of Si Nanocrystals by Simultaneously Doping n- and p-Type Impurities. *Appl. Phys. Lett.* **2004**, *85*, 1158–1160.
- (18) Nakamura, T.; Adachi, S.; Fujii, M.; Miura, K.; Yamamoto, S. Phosphorus and Boron Codoping of Silicon Nanocrystals by Ion Implantation: Photoluminescence Properties. *Phys. Rev. B* **2012**, *045441*.
- (19) Gabriel, M. M.; Kirschbrown, J. R.; Christesen, J. D.; Pinion, C. W.; Zigler, D. F.; Grumstrup, E. M.; Mehl, B. P.; Cating, E. E. M.; Cahoon, J. F.; Papanikolas, J. M. Direct Imaging of Free Carrier and Trap Carrier Motion in Silicon Nanowires by Spatially-Separated Femtosecond Pump-Probe Microscopy. *Nano Lett.* **2013**, *13*, 1336–1340.

- (20) De Ranieri, E. Ultrafast Microscopy: Charge Carriers Caught on Camera. *Nat. Nanotechnol.* **2013**, *13*, 1336–1340.
- (21) Webb, S. P.; Iordanov, T.; Hammes-Schiffer, S. Multiconfigurational Nuclear-Electronic Orbital Approach: Incorporation of Nuclear Quantum Effects in Electronic Structure Calculations. *J. Chem. Phys.* **2002**, *117*, 4106–4118.
- (22) Hammes-Schiffer, S. Avoiding the Born-Oppenheimer Separation Between Electrons and Nuclei: Explicitly Correlated Wavefunctions and Multicomponent Density Functional Theory. *Abstracts of Papers of the American Chemical Society* **2011**, 242.
- (23) Tempel, D. G.; Aspuru-Guzik, A. Relaxation and Dephasing in Open Quantum Systems Time-Dependent Density Functional Theory: Properties of Exact Functionals From an Exactly-Solvable Model System. *Chem. Phys.* **2011**, *391*, 130–142.
- (24) Parkhill, J. A.; Tempel, D. G.; Aspuru-Guzik, A. Exciton Coherence Lifetimes from Electronic Structure. *J. Chem. Phys.* **2012**, *136*, 9.
- (25) Rego, L. G. C.; Batista, V. S. Quantum Dynamics Simulations of Interfacial Electron Transfer in Sensitized TiO₂ Semiconductors. *J. Am. Chem. Soc.* **2003**, *125*, 7989–7997.
- (26) Kilin, D. S.; Micha, D. A. Relaxation of Photoexcited Electrons at a Nanostructured Si(111) Surface. *J. Phys. Chem. Lett.* **2010**, *1*, 1073–1077.
- (27) Kilina, S. V.; Craig, C. F.; Kilin, D. S.; Prezhdo, O. V. Ab Initio Time-Domain Study of Phonon-Assisted Relaxation of Charge Carriers in a PbSe Quantum Dot. *J. Phys. Chem. C* **2007**, *111*, 4871–4878.
- (28) Kilina, S. V.; Kilin, D. S.; Prezhdo, O. V. Breaking the Phonon Bottleneck in PbSe and CdSe Quantum Dots: Time-Domain Density Functional Theory of Charge Carrier Relaxation. *ACS Nano* **2009**, *3*, 93–99.
- (29) Kilina, S. V.; Kilin, D. S.; Prezhdo, V. V.; Prezhdo, O. V. Theoretical Study of Electron-Phonon Relaxation in PbSe and CdSe Quantum Dots: Evidence for Phonon Memory. *J. Phys. Chem. C* **2011**, *115*, 21641–21651.
- (30) Tully, J. C. Molecular Dynamics with Electronic Transitions. *J. Chem. Phys.* **1990**, *93*, 1061–1071.
- (31) Fernandez-Alberti, S.; Kleiman, V. D.; Tretiak, S.; Roitberg, A. E. Nonadiabatic Molecular Dynamics Simulations of the Energy Transfer between Building Blocks in a Phenylene Ethynylene Dendrimer. *J. Phys. Chem. A* **2009**, *113*, 7535–7542.
- (32) Fernandez-Alberti, S.; Kleiman, V. D.; Tretiak, S.; Roitberg, A. E. Unidirectional Energy Transfer in Conjugated Molecules: The Crucial Role of High-Frequency C C Bonds. *J. Phys. Chem. Lett.* **2010**, *1*, 2699–2704.
- (33) Nelson, T.; Fernandez-Alberti, S.; Chernyak, V.; Roitberg, A. E.; Tretiak, S. Nonadiabatic Excited-State Molecular Dynamics Modeling of Photoinduced Dynamics in Conjugated Molecules. *J. Phys. Chem. B* **2011**, *115*, 5402–5414.
- (34) Nelson, T.; Fernandez-Alberti, S.; Chernyak, V.; Roitberg, A. E.; Tretiak, S. Nonadiabatic Excited-State Molecular Dynamics: Numerical Tests of Convergence and Parameters. *J. Chem. Phys.* **2012**, *136*, 5.
- (35) Redfield, A. G. On the Theory of Relaxation Processes. *IBM J. Res. Dev.* **1957**, *1*, 19–31.
- (36) Egorova, D.; Thoss, M.; Domcke, W.; Wang, H. B. Modeling of Ultrafast Electron-Transfer Processes: Validity of Multilevel Redfield Theory. *J. Chem. Phys.* **2003**, *119*, 2761–2773.
- (37) Pollard, W. T.; Friesner, R. A. Solution of The Redfield Equation for the Dissipative Quantum Dynamics of Multilevel Systems. *J. Chem. Phys.* **1994**, *100*, 5054–5065.
- (38) Pollard, W. T.; Felts, A. K.; Friesner, R. A. The Redfield Equation in Condensed-Phase Quantum Dynamics. *Adv. Chem. Phys.* **1996**, *93*, 77–134.
- (39) Jean, J. M.; Friesner, R. A.; Fleming, G. R. Application of a Multilevel Redfield Theory to Electron Transfer in Condensed Phases. *J. Chem. Phys.* **1992**, *96*, 5827–5842.
- (40) Sundstrom, V.; Pullerits, T.; van Grondelle, R. Photosynthetic Light-Harvesting: Reconciling Dynamics and Structure of Purple Bacterial LH2 Reveals Function of Photosynthetic Unit. *J. Phys. Chem. B* **1999**, *103*, 2327–2346.
- (41) Kuhn, O.; May, V.; Schreiber, M. Dissipative Vibrational Dynamics in a Curve-Crossing System. *J. Chem. Phys.* **1994**, *101*, 10404–10415.
- (42) Davis, W. B.; Wasielewski, M. R.; Ratner, M. A.; Mujica, V.; Nitzan, A. Electron Transfer Rates in Bridged Molecular Systems: A Phenomenological Approach to Relaxation. *J. Phys. Chem. A* **1997**, *101*, 6158–6164.
- (43) Arlund, D.; Kilin, S. Y.; Nizovtsev, A. P.; Onishchenko, N. S. Statistics of Dephasing Perturbations and Relaxational Processes in a High-Power Optic Field - Application to Free Induction Decay. *J. Opt. Soc. Am. B* **1986**, *3*, 587–594.
- (44) Ramirez, J. J.; Kilin, D. S.; Micha, D. A. Optical properties of the Si(111):H surface with Adsorbed Ag Clusters. *Int. J. Quantum Chem.* **2009**, *109*, 3694–3704.
- (45) Arlund, D.; Micha, D. A.; Kilin, D. S. Computational Studies of the Optical Properties of Silicon Compounds Bonding to Silver Atoms and with Group III and V Substituents. *Int. J. Quantum Chem.* **2010**, *110*, 3086–3094.
- (46) Lajoie, T. W.; Ramirez, J. J.; Kilin, D. S.; Micha, D. A. Optical Properties of Amorphous and Crystalline Silicon Surfaces Functionalized with Ag(n) Adsorbates. *Int. J. Quantum Chem.* **2010**, *110*, 3005–3014.
- (47) Ramirez, J. J.; Kilin, D. S.; Micha, D. A. Electronic Structure and Optical Absorbance of Doped Amorphous Silicon Slabs. *Int. J. Quantum Chem.* **2012**, *112*, 300–313.
- (48) Chen, J.; Schmitz, A.; Kilin, D. S. Computational Simulation of the p-n Doped Silicon Quantum Dot. *Int. J. Quantum Chem.* **2012**, *112*, 3879–3888.
- (49) Hohenberg, P.; Kohn, W. Inhomogeneous Electron Gas. *Phys. Rev. B* **1964**, *136*, B864–B871.
- (50) Kohn, W.; Sham, L. J. Self-Consistent Equations Including Exchange and Correlation Effects. *Phys. Rev.* **1965**, *140*, A1133–A1138.
- (51) Perdew, J. P.; Burke, K.; Ernzerhof, M. Generalized Gradient Approximation Made Simple. *Phys. Rev. Lett.* **1996**, *77*, 3865–3868.
- (52) Kresse, G.; Furthmüller, J. Efficient Iterative Schemes for Ab Initio Total-Energy Calculations Using a Plane-Wave Basis Set. *Phys. Rev. B* **1996**, *54*, 11169–11186.
- (53) Vanderbilt, D. Soft Self-Consistent Pseudopotentials in a Generalized Eigenvalue Formalism. *Phys. Rev. B* **1990**, *41*, 7892–7895.
- (54) Rohlfing, M.; Louie, S. G. Excitonic Effects and the Optical Absorption Spectrum of Hydrogenated Si Clusters. *Phys. Rev. Lett.* **1998**, *80*, 3320–3323.
- (55) Ekimov, A. I.; Efros, A. L.; Onushchenko, A. A. Quantum Size Effect in Semiconductor Microcrystals (reprinted from *Solid State Commun.* **1985**, *56*, 921–924). *Solid State Commun.* **1993**, *88*, 947–950.
- (56) Kilina, S.; Ivanov, S.; Tretiak, S. Effect of Surface Ligands on Optical and Electronic Spectra of Semiconductor Nanoclusters. *J. Am. Chem. Soc.* **2009**, *131*, 7717–7726.
- (57) Mikhailov, I. A.; Chen, J.; Schmitz, A.; Kilin, D. S. Dynamics of Charge Transfer at p-n Junction. *Prepr. - Am. Chem. Soc., Div. Energy Fuels* **2012**, *57*, 527.
- (58) Takagahara, T.; Takeda, K. Excitonic Exchange Splitting and Stokes Shift in Si Nanocrystals and Si Clusters. *Phys. Rev. B* **1996**, *53*, R4205–R4208.
- (59) Hirao, M.; Uda, T. First Principles Calculation of The Optical Properties and Stability of Hydrogenated Silicon Clusters. *Int. J. Quantum Chem.* **1994**, *52*, 1113–1119.
- (60) Zhang, R. Q.; De Sarkar, A.; Niehaus, T. A.; Frauenheim, T. Excited State Properties of Si Quantum Dots. *Phys. Status Solidi B* **2012**, *249*, 401–412.
- (61) Inerbaev, T. M.; Kilin, D. S.; Hoefelmeyer, J. D. Atomistic Simulation of Dissipative Charge Carrier Dynamics for Photocatalysis. *MRS Proc.* **2012**, *1390*, mrsf11-1390i03-03.

(62) Inerbaev, T. M.; Hoefelmeyer, J. D.; Kilin, D. S. Photoinduced Charge Transfer from Titania to Surface Doping Site. *J. Phys. Chem. C* **2013**, *117*, 9673–9692.

(63) Jensen, S.; Kilin, D. Dissipative Dynamics of Charge in Silver Doped TiO₂ Anatase (100) Surface. In *Nanotechnology for Sustainable Energy*; ACS Symposium Series 1140; American Chemical Society: Washington, DC, 2013; Chapter 8, pp 187–218, Chapter DOI: 10.1021/bk-2013-1140.ch008.

(64) Duncan, W. R.; Prezhdo, O. V. Theoretical Studies of Photoinduced Electron Transfer in Dye-Sensitized TiO₂. *Annu. Rev. Phys. Chem.* **2007**, *58*, 143–184.

(65) Hyeon-Deuk, K.; Madrid, A. B.; Prezhdo, O. V. Symmetric Band Structures and Asymmetric Ultrafast Electron and Hole Relaxations in Silicon and Germanium Quantum Dots: Time-Domain Ab Initio Simulation. *Dalton Trans.* **2009**, *0*, 10069–10077.

(66) Kryjevski, A. B.; Kilin, D. S.; Kilina, S. V. Amorphous Silicon Nanomaterials: Quantum Dots Versus Nanowires. *J. Renewable Sustainable Energy*, **2013**, *5*, 043120–16.

(67) Mavros, M. G.; Micha, D. A.; Kilin, D. S. Optical Properties of Doped Silicon Quantum Dots with Crystalline and Amorphous Structures. *J. Phys. Chem. C* **2011**, *15*, 19529–19537.

(68) Ramdas, A. K.; Rodriguez, S. Spectroscopy of the Solid State Analogues of the Hydrogen Atom: Donors and Acceptors in Semiconductors. *Rep. Prog. Phys.* **1981**, *44*, 1297–1387.